Title

Dual-stage nanopositioner augmented with feedforward control

Journal

IFAC-PapersOnLine, 55(27)

ISSN

2405-8963

Authors

Pyle, Kenneth E

M'Closkey, Robert T

Publication Date

2022

DOI

10.1016/j.ifacol.2022.10.523

Dual-stage nanopositioner augmented with feedforward control

Kenneth E. Pyle * **Robert T. M'Closkey** **

* *University of California, Los Angeles, CA 90095 USA (e-mail: kennypyle@ucla.edu).*
** *University of California, Los Angeles, CA 90095 USA (e-mail: rtm@seas.ucla.edu).*

Abstract:
A piezoelectric walking stage is retrofitted with a secondary stage for precisely tracking ramp position references. Fine motion control of the secondary stage shuttle is achieved using a voice coil actuator to correct for small, periodic deviations in position produced by the walking motion of the piezoelectric drive modules. The shuttle position tracking error is more than an order of magnitude smaller than the walking stage error for velocities less than 1.0 mm/s, however, the shuttle error remains dominated by harmonics of the walking stage stepping frequency. A feedforward controller using a modulated-demodulated implementation is designed to augment the high-bandwidth (300 Hz) shuttle controller to reject three dominant disturbance modes. When the system is tracking a 1.0 mm/s position ramp reference, the modulated-demodulated controller reduces the RMS shuttle position error from 44 to 21 nm. The reported system is under development to meet the scanning requirements of spaceborne Fourier Transform spectrometers.

Keywords: Motion and Vibration Control

1. INTRODUCTION

A dual-stage system for precisely tracking ramp position references is proposed. The system is designed to meet the requirements of spaceborne Fourier Transform spectrometers, which include compact size, vacuum compatibility, and rigorous position-tracking capability over a range of several centimeters [Saptari, 2004]. A piezoelectric walking stage is selected to serve as the base stage due to its long working stroke and nanometer-level point-to-point positioning capabilities. When the walking stage is in motion, however, intermittent contact of the piezoelectric drive elements with the runner perturb the stage position from the desired reference trajectory. While tracking capabilities can be improved by properly designing the voltage profiles that actuate the drive modules [Merry et al., 2009] and equalizing variations in local gain that are a function of the step "phase" [Merry et al., 2014], the walking stage is incapable of regulating the stage position to the level required for the scanning operation of Fourier-transform spectrometers. Thus, a short-stoke, fine-motion secondary stage is employed.

Compact examples of dual-stage systems have been demonstrated in which a stiff, fine motion piezoelectric actuator is mounted to a coarse, long-stroke linear bearing or slideway [Buice et al., 2009, Chassagne et al., 2007, Kramar, 2005, Sinno et al., 2007]. In Fourier transform spectrometers, however, using a low-stiffness secondary stage is advantageous since the weak elastic coupling between the two stages passively attenuates disturbances transmitted from the primary stage to the secondary stage. Such disturbances are mitigated further by using a voice coil actuator to drive the secondary stage's movable shuttle. A linear, high-bandwidth feedback controller regulates the shuttle position, however, when the dual-stage system operates at a constant velocity, periodic errors in the shuttle position persist at harmonics of the walking stage's stepping frequency. Various control techniques, such as iterative learning control, have been shown to reduce repetitive errors in nanopositioning systems [Parmar et al., 2014, Steinbuch and van de Molengraft, 2000]. Alternatively, modulated-demodulated control, or adaptive feedforward cancellation, has been demonstrated to improve the rejection of periodic disturbances over a wide array applications, including diamond turning machines and superconducting radio frequency cavities [Byl et al., 2005, Hendrickson and M'Closkey, 2012, Kandil et al., 2005]. This technique works by shifting the high frequency error components down to baseband, integrating for asymptotic reference tracking/disturbance rejection, and modulating the signals back to their high frequency components. A single modulated-demodulated controller improves performance only at a specific frequency, though a family of controllers can be organized in parallel to reduce repetitive errors over a set of frequencies.

This paper discusses the motivation for and implementation of modulated-demodulated controllers with static phase compensation over a select set of constant velocity trajectories. The linear controllers around the walking stage and shuttle loops remain intact while three modulated-demodulated compensators are added in parallel to the existing shuttle controller. It is shown that the inclusion of the modulated-demodulated controllers reduce RMS tracking errors in the shuttle by a factor of 2 as reference speeds approach 1.0 mm/s.

The paper is organized as follows: Sec. 2 describes the dual-stage plant; Sec. 3 introduces the baseline feedback controller and presents the shortcomings of the shuttle controller; Sec. 4 discusses the design and architecture of the modulated-

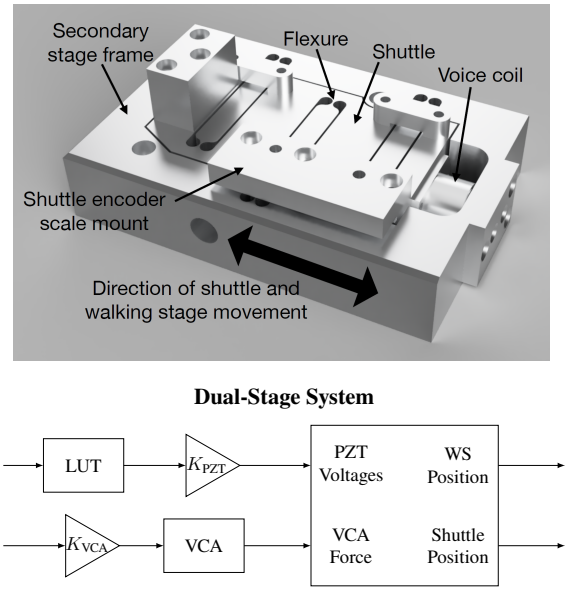

Fig. 1. **Top:** Render of the secondary stage subsystem that bolts to a Physik Instrumente N-565 linear stage. **Bottom:** Block diagram of the two-input/two-output plant.

demodulated controller; Sec. 5 presents tracking error results of ramp position references using the modulated-demodulated controller; Sec. 6 concludes the paper.

2. SYSTEM DESCRIPTION

The dual-stage system consists of a secondary stage whose frame is affixed to a Physik Instrumente N-565 linear walking stage (WS). The walking stage has a linear translational stroke of 52 mm and is integrated with a 0.5 nm-resolution encoder. The stepping drive mechanism features two sets of piezoelectric bimorph elements (PZTs) that are controlled by four voltages that specify the feed and clamping associated with each set. The voltage profiles are based on those in [Merry et al., 2009] and defined in a look-up-table (LUT). The input to the LUT, u_1, is a non-dimensional phase. Since the profiles are periodic, the LUT can be interpreted as applying a modulo operation on its input, with phase interval $[0, 1000]$. The output of the LUT drives a set of voltage buffers, given by K_{PZT} in Fig. 1, that scale the profiles to the voltage range of the PZTs. One cycle through the LUT moves the stage about 8 μm and the lowest frequency mode of the walking stage is approximately 800 Hz.

The secondary stage, shown in Fig. 1, is fabricated from aluminum using electrodischarge machining. Three sets of flexures permit translational motion of the shuttle collinear to the walking stage's degree of freedom. The shuttle mass is 0.09 kg, the flexure spring rate is approximately 1900 N/m, and the lowest frequency mode of the secondary stage is the shuttle translational mode at 24 Hz. The relatively low stiffness of the shuttle flexures is instrumental in passively rejecting disturbances imparted on the shuttle by the walking stage. The secondary stage is instrumented with a Sensata LA05-05 voice coil actuator (VCA) that exerts forces between the shuttle and frame. The VCA coil is mounted to the secondary stage frame and the magnet is affixed to the shuttle. The VCA magnet displacement is a very linear function of u_2 for the experiments discussed in Secs. 3 and 5 due to the fact that the shuttle moves less than 1 μm relative to the frame, even though the shuttle-frame

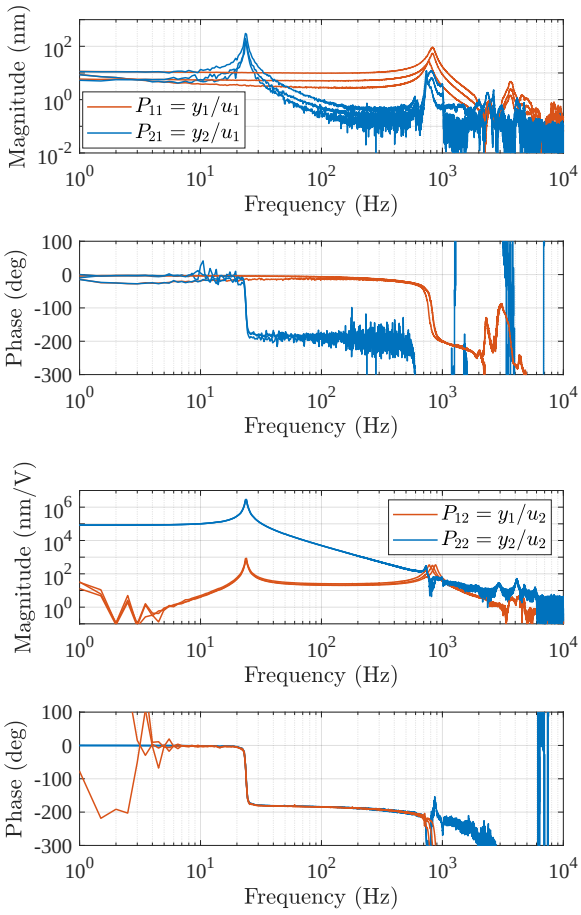

Fig. 2. **Top:** Open-loop empirical frequency responses to a walking stage phase dither input about three nominal LUT phases. **Bottom:** Empirical frequency responses to the voice coil voltage input about the same three nominal LUT phases. The errors in the estimates of P_{12} at low frequencies can be attributed to low output signal power and can be ignored.

gaps are 500 μm when the system is at rest. The K_{VCA} gain of Fig. 1 represents the voice coil voltage amplifier and the scale factor of the voltage u_2 to the voice coil force is 0.162 N/V. A Celera Mercury II 6800 optical encoder provides 1.22 nm resolution of the shuttle's position. The encoder readhead (not shown in Fig. 1) is fixed to the same optical bench as the base of the walking stage so that the global position of the shuttle is measured.

The dual-stage plant, P, is a two-input/two-output system. The inputs correspond to the LUT phase, u_1, and the voltage supplied to the VCA driving amplifier, u_2. The output variables are the walking stage and shuttle position measurements, y_1 and y_2, respectively. Empirical frequency response models of the open-loop plant are provided in Fig. 2. These estimates are generated about nominal look-up-table phases, ϕ_0, using broadband, gaussian stimulus signals. The three separate models for each channel correspond to specific values of ϕ_0 that are chosen to represent the extremes in gain and resonant frequency variations in the y_1/u_1 and y_2/u_1 channels. These variations can be attributed to the fact that the orientation of the PZTs and their authority over stage motion is ϕ_0-dependent. In the P_{21} channel, passive isolation of the shuttle from the stage is

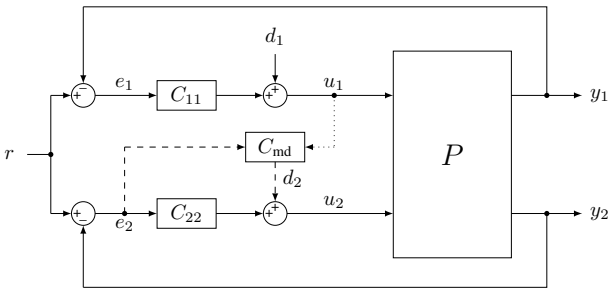

Fig. 3. Closed-loop block diagram. Sec. 4 discussed the modulated-demodulated controller, C_{md}.

evident above 34 Hz. The P_{12} frequency response indicates that the VCA does drive the stage, though at much lower authority than the shuttle below the walking stage mode.

3. LIMITATIONS OF THE BASELINE CONTROLLER

The baseline feedback controller employs a two-input/two-output diagonal topology. It regulates the walking stage with low bandwidth to asymptotically track ramp position references. The shuttle, however, has a 300 Hz closed-loop bandwidth that attenuates disturbances imparted on the shuttle by walking stage motion. The baseline control elements are given by

$$C_{11} = 2(s+2)/s^2,$$
$$C_{22} = \left(K_{\text{P}} + K_{\text{I}}\frac{1}{s} + K_{\text{D}}\frac{s}{s+\omega_{\text{co}}}\right) N_1(s)N_2(s),$$

where $N_1(s)$ and $N_2(s)$ are 740 Hz and 4.035 kHz notch filters, respectively, and ω_{co} represents the high frequency corner of the differentiation filter.

The closed-loop complementary sensitivity functions of both the walking stage and shuttle loops are estimated by applying a broadband, gaussian reference signal to the feedback system of Fig. 3 (excluding C_{md}) and measuring the walking stage and shuttle encoder signals. The empirical results are shown in Fig. 4 and indicate that the dual-stage system provides a significant improvement in tracking performance over the walking stage alone. The walking stage provides poor reference tracking above 1 Hz and its performance is dependent on ϕ_0. The shuttle bandwidth, however, is 300 Hz for all PZT orientations.

Time-domain tests are also performed using ramp position references corresponding to $\{0.1, 0.2, 0.5, 1.0\}$ mm/s velocities. The RMS position tracking errors of the walking stage and shuttle at each speed are provided in Table 1. The addition of the shuttle loop reduces the tracking error by at least an order of magnitude for all speeds below 1.0 mm/s, with the position tracking capabilities appearing to improve as the velocity diminishes. Time-domain plots of the walking stage and shuttle tracking errors at speeds of 0.2 and 1.0 mm/s are shown in Figs. 5 and 6, respectively.

While the peak-to-peak tracking errors of Figs. 5 and 6 have been significantly reduced in the shuttle, periodic components are clearly present in e_2 when the system is operating at a constant velocity. In fact, the spectra of the shuttle error signals, shown in Fig. 7 for the 0.2 and 1.0 mm/s speeds, confirm that the tracking errors are dominated by only a few frequency components. These dominant modes are the result of disturbances imparted on the shuttle by the intermittent contact of the PZTs with the runner and are directly related to the

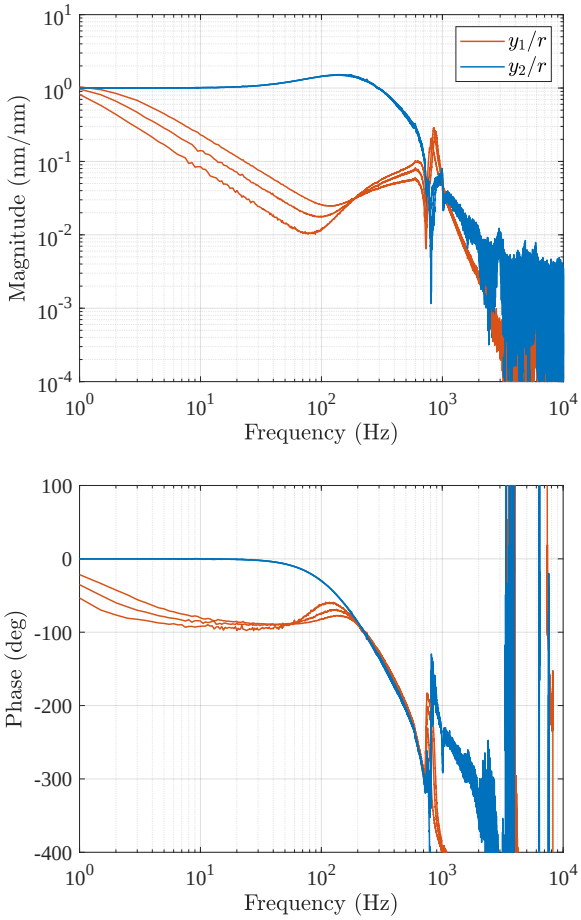

Fig. 4. Measured closed-loop complementary sensitivity functions of the walking stage and shuttle loops.

Table 1. Walking Stage and Shuttle RMS Errors

Velocity (mm/s)	Walking Stage e_1 (nm)	Shuttle, $C_{\text{md}} = 0$ e_2 (nm)
0.1	213	2.7
0.2	216	5.2
0.5	238	13.0
1.0	344	43.9

walking stage velocity. Since one cycle through the LUT moves the walking stage about 8 μm, the average rate at which u_1 scans through the LUT for a given reference speed can be computed. For example, when the walking stage is moving at a constant velocity of 1.0 mm/s, the PZT voltages operate at a frequency of about 128 Hz. Given that each set of PZT "legs" contacts the runner once each period through the LUT, disturbances imparted on the shuttle by the walking stage are expected with a fundamental harmonic of twice the frequency of the PZT voltages. For the 1.0 mm/s case, this corresponds to 256 Hz, which matches the error spectrum of Fig. 7.

4. MODULATED-DEMODULATED CONTROL FILTER

These periodic error signals motivate the use of a feedforward scheme to reject disturbances at specific frequencies. Numerous feedforward implementations are available for reducing periodic errors, however, modulated-demodulated control is well-suited for rejecting the harmonic disturbances experienced by

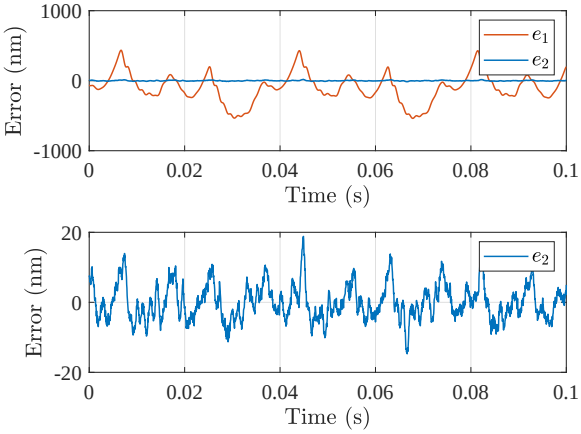

Fig. 5. **Top:** Walking stage and shuttle position errors for a 0.2 mm/s ramp position reference. **Bottom:** Shuttle error detail.

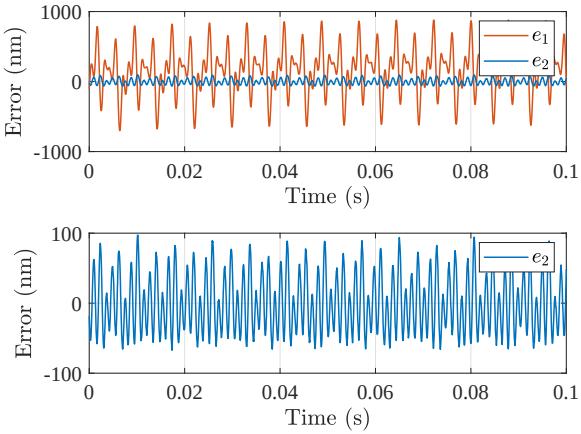

Fig. 6. **Top:** Walking stage and shuttle position for a 1.0 mm/s ramp position reference. **Bottom:** Shuttle error detail.

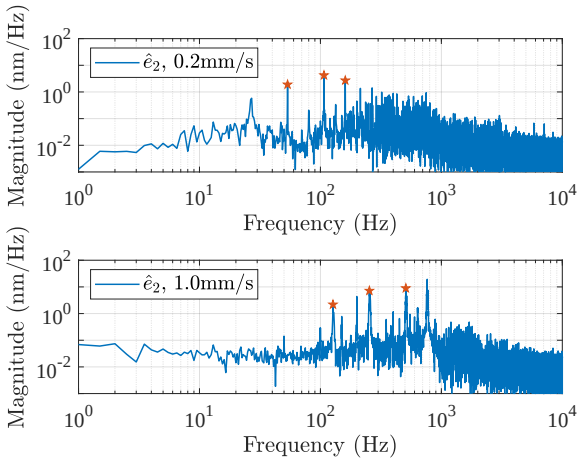

Fig. 7. Spectra of the closed-loop shuttle position error when the walking stage is moving at 0.2 and 1.0 mm/s. The modes highlighted by the $\star$ symbols will be rejected by the modulated-demodulated controllers.

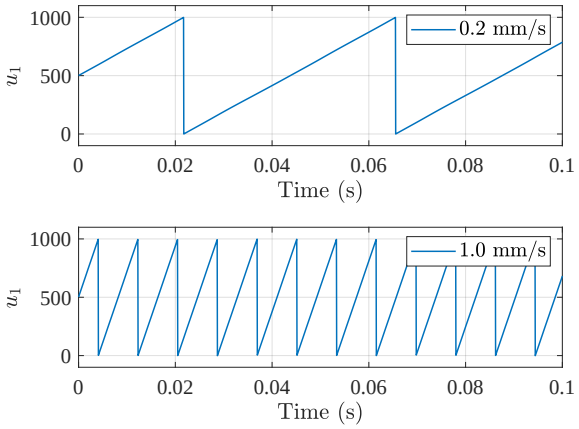

Fig. 8. LUT input phase, u_1, during closed-loop operation using 0.2 and 1.0 mm/s ramp position references.

the shuttle given that the periodicity of e_2 is a direct consequence of the periodicity of u_1. The u_1 signal, shown in Fig. 8, is a very linear function of time and provides a convenient time-base for generating harmonic signals. Regulation of specific harmonics is easily achieved by appropriately scaling this time-base. From Fig. 7, the dominant components of the shuttle error occur at the first, second, and third harmonics of the PZT-runner contact disturbances. These three harmonics appear to dominate e_2 for all ramp position references in the $[0.1, 1.0]$ mm/s range. Thus, three modulated-demodulated controllers are added in parallel to C_{22} to reject disturbances at the first three harmonics of the shuttle error at each speed. The sum of these three controllers represent the modulated-demodulated control filter of Fig. 3, i.e. $C_{\text{md}} = C_{\text{md},1} + C_{\text{md},2} + C_{\text{md},3}$.

The architecture of a single modulated-demodulated controller is shown in Fig. 9 and its corresponding transfer function is given by

$$C_{\text{md},j} = K_j \frac{a_j s + b_j \omega_{0,j}}{s^2 + \omega_{0,j}^2}, \quad j = 1, 2, 3$$

where $\omega_{0,j}$ is the "rejection" frequency and is related to u_1 as explained below. The pertinent transfer function seen from the perspective of C_{md}, e_2/d_2, is provided in Fig. 10 and is useful in specifying the a_j and b_j coefficients that define the phase of the controller. These terms are constrained by the equation $a_j^2 + b_j^2 = 1$ and, due to the positive feedback convention, are selected so that the phase of the loop gain $e_2/d_2 \cdot C_{\text{md}}$ is $180°$ at the rejection frequency. The e_2/d_2 transfer function is shown to vary widely in phase over the frequency band within which dominant disturbance harmonics fall for references in the 0.1 to 1.0 mm/s range. Thus, a single set of controller coefficients is inadequate for the velocity range of interest and separate modulated-demodulated controllers are designed for each speed. Each individual modem controller's gain, K_j, is chosen so that the controller has a time constant of 0.125 s.

In order to generate the sinusoids necessary for modulation/demodulation, trigonometric functions are applied to scaled versions of the LUT input phase, i.e. the input to the sin and cos blocks of Fig. 9 is the argument of the corresponding trigonometric function. This is made possible by the fact that u_1 is a very linear function of time and provides the benefit of producing sinusoids at exactly the frequencies of the major disturbance components. The phase gain, G, in Fig. 9, is given by $n_j \times$

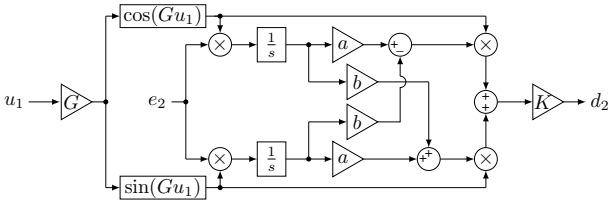

Fig. 9. Block diagram of a single modulated/demodulated controller. Three of these controllers in parallel comprise the C_{md} control filter of Fig 3.

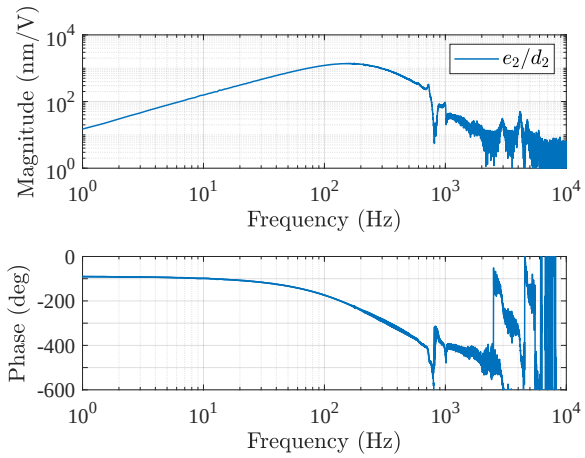

Fig. 10. Frequency response from the perspective of C_{md}.

Table 2. Shuttle RMS Tracking Errors

Velocity (mm/s)	Shuttle, $C_{\text{md}} = 0$ e_2 (nm)	Shuttle, $C_{\text{md}} \neq 0$ e_2 (nm)
0.1	2.7	2.3
0.2	5.2	3.5
0.5	13.0	7.1
1.0	43.9	21.2

$2\pi/1000$, where $n_j = \{2, 4, 6\}$ so that disturbances located at the second, fourth, and sixth harmonics of the PZT voltages–or the first, second, and third shuttle error harmonics–are rejected. In order to avoid exciting the plant mode near 800 Hz an exception occurs in the 1.0 mm/s case, where $n_j = \{1, 2, 4\}$ so that the modulated-demodulated control filter rejects components located at the "half-harmonic" at 128 Hz instead of the third shuttle error harmonic at 768 Hz. The $2\pi/1000$ term converts the non-dimensional LUT phase into radians.

The robustness of the new closed-loop system is analyzed using the structured singular value applied to simultaneous multiplicative input perturbations. This analysis is not included here for brevity, though it indicates that the dual-stage system is robustly stable to perturbation magnitudes of less than 0.5 about all nominal LUT phases. These results are essentially identical whether or not the modulated-demodulated controllers are introduced to the feedback loop since C_{md} has a negligible impact on the shuttle loop gain outside of tight frequency bands surrounding the rejection frequencies. These stability margins are deemed acceptable and the modulated-demodulated control filter is implemented.

5. EXPERIMENTAL RESULTS

Closed-loop testing is performed using the same ramp position references that correspond to $\{0.1, 0.2, 0.5, 1.0\}$ mm/s velocities. Time-domain examples of the shuttle tracking error are graphed in Fig. 11 and the RMS position tracking errors of the shuttle with and without C_{md} are provided in Table 2.

The addition of the modulated-demodulated control filter to the feedback loop reduces RMS tracking errors by a factor of 2 as the stage velocity approaches 1.0 mm/s and appears to have a greater effect on system performance as the velocity increases. This can be attributed to the performance of the C_{22} controller. At slower speeds, the fundamental harmonic of disturbances imparted on the shuttle shifts to lower frequencies. For a 0.1 mm/s reference, the fundamental disturbance harmonic is about 25 Hz. All three of the modes rejected by the C_{md} controller easily fall within the C_{22} controller's 300 Hz bandwidth, so they have already experienced large attenuation. At reference speeds of 1.0 mm/s, on the other hand, the dominant components of walking stage disturbances occur near or above the $P_{22}C_{22}$ gain crossover, so disturbance rejection is less effective. When C_{md} is introduced to the feedback loop, these components that are only marginally attenuated by C_{22} are rejected. At speeds below 0.1 mm/s the modulated-demodulated control filter provides essentially no improvement in reference tracking, however, the performance capabilities at speeds in this range are dependent on encoder (1.22 nm-resolution) and VCA (1.27 nm/bit DC resolution) quantization. Periodic tracking errors do remain after the modulated-demodulated controllers are implemented, though these errors are riddled with high-frequency components that lie in a neighborhood of the 800 Hz walking stage mode and are not tied to the walker's velocity. These errors are exacerbated in the 1.0 mm/s case since the third harmonic of e_2 aligns closely with this walking stage mode.

Empirical closed-loop sensitivity functions are generated by capturing the u_2/d_2 frequency response function and are provided in Fig. 12 for ramp position references corresponding to speeds of 0.2 and 1.0 mm/s. The low frequency errors are the result of low power in the u_2 signal below 30 Hz. The lobes in the plots correspond to the rejection frequencies of the modulated-demodulated controllers and both sensitivity functions have a peak magnitude of about 2.

Small variations in PZT operating frequency, and thus disturbance harmonics, do occur while the walking stage moves at a constant velocity over its entire stroke. The fact that the control filter's modulation/demodulation signals are generated from u_1, however, yield control signals at exact harmonics of the instantaneous PZT operating frequency. Thus, the performance capabilities of C_{md} are not susceptible to perturbations in disturbance frequency. Variations in the phase of the e_2/d_2 transfer function due to dependency on ϕ_0, however, do make the filter's performance somewhat susceptible to errors in phase since the a_j and b_j coefficients of the controller transfer functions are computed from empirical models of e_2/d_2.

6. CONCLUSION

A dual-stage system is developed to meet the continuous scan requirements of spaceborne Fourier Transform spectrometers. A low-bandwidth controller is implemented for the piezoelectric walking stage "base" to asymptotically track ramp position references. Meanwhile, weak elastic coupling between the two

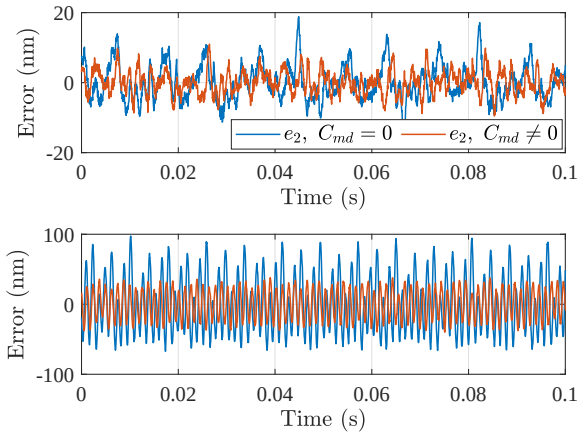

Fig. 11. Shuttle position errors with and without the modulated-demodulated control filter. **Top:** 0.2 mm/s ramp position reference. **Bottom:** 1.0 mm/s ramp position reference.

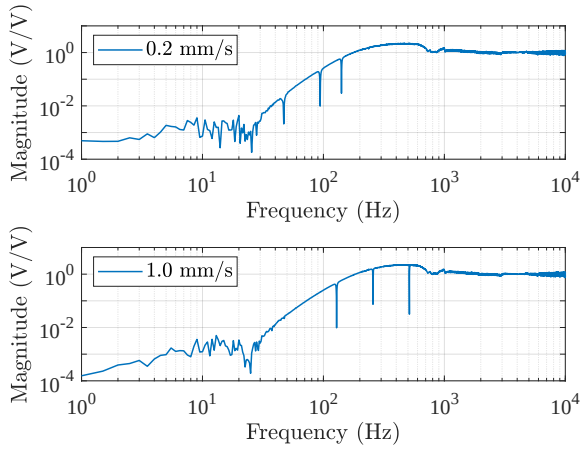

Fig. 12. Empirical closed-loop sensitivity function of the shuttle loop. **Top:** C_{md} designed for a 0.2 mm/s ramp position reference. **Bottom:** C_{md} designed for a 1.0 mm/s ramp position reference.

stages and a high-bandwidth linear shuttle controller effectively attenuate disturbances transmitted from the stage to the shuttle below 300 Hz. Closed-loop results indicate, however, that the shuttle tracking error remains riddled with periodic components at harmonics of the walking stage operating frequency. Three dominant harmonics are rejected by including three modulated-demodulated controllers in parallel with the high-bandwidth shuttle controller. The modulation/demodulation sinusoids are generated using the walking stage LUT input so that the controller outputs exactly match the error harmonics in frequency. Including the modem controllers in the feedback loop reduces the RMS shuttle error by a factor of 2 as the velocity approaches 1.0 mm/s.

ACKNOWLEDGEMENTS

The authors thank the Jet Propulsion Laboratory SURP program for supporting this research and Fadi Rafidi for manufacturing the secondary stage.

REFERENCES

Buice, E.S., Otten, D., Yang, R.H., Smith, S.T., Hocken, R.J., and Trumper, D.L. (2009). Design evaluation of a single-axis precision controlled positioning stage. *Precision Engineering*, 33(4), 418–424.

Byl, M.F., Ludwick, S.J., and Trumper, D.L. (2005). A loop shaping perspective for tuning controllers with adaptive feedforward cancellation. *Precision Engineering*, 29(1), 27–40.

Chassagne, L., Wakim, M., Xu, S., Topçu, S., Ruaux, P., Juncar, P., and Alayli, Y. (2007). A 2D nano-positioning system with sub-nanometric repeatability over the millimetre displacement range. *Meas. Sci. Technol.*, 18(11), 3267–3272.

Hendrickson, C. and M'Closkey, R.T. (2012). Phase compensation strategies for modulated-demodulated control with application to pulsed jet injection. *Journal of Dynamic Systems, Measurement, and Control*, 134(1), 011024.

Kandil, T., Khalil, H., Vincent, J., Grimm, T., Hartung, W., Popielarski, J., York, R., and Seshagiri, S. (2005). Adaptive feedforward cancellation of sinusoidal disturbances in superconducting rf cavities. *Nucl. Instrum. Methods in Phys. Res.*, 550(3), 514–520.

Kramar, J.A. (2005). Nanometre resolution metrology with the molecular measuring machine. *Meas. Sci. Technol.*, 16(11), 2121–2128.

Merry, R.J.E., de Kleijn, N.C.T., van de Molengraft, M.J.G., and Steinbuch, M. (2009). Using a walking piezo actuator to drive and control a high-precision stage. *IEEE/ASME Trans. Mechatronics*, 14(1), 21–31.

Merry, R.J.E., Holierhoek, J.L., van de Molengraft, M.J.G., and Steinbuch, M. (2014). Gain scheduling control of a walking piezo actuator. *IEEE/ASME Trans. Mechatronics*, 19(3), 954–962.

Parmar, G., Barton, K., and Awtar, S. (2014). Large dynamic range nanopositioning using iterative learning control. *Precision Engineering*, 38(1), 48–56.

Saptari, V. (2004). *Fourier-Transform Spectroscopy Instrumentation Engineering*, volume TT61. SPIE Press.

Sinno, A., Ruaux, P., Chassagne, L., Topçu, S., Alayli, Y., Lerondel, G., Blaize, S., Bruyant, A., and Royer, P. (2007). Enlarged atomic force microscopy scanning scope: Novel sample-holder device with millimeter range. *Rev. Sci. Instrum.*, 78(9), 1–7.

Steinbuch, M. and van de Molengraft, R. (2000). Iterative learning control of industrial motion systems. *IFAC Proceedings Volumes*, 33(26), 899–904.